Asymmetric modification of the magnetic proximity effect in Pt/Co/Pt trilayers by the insertion of a Ta buffer layer

Ankan Mukhopadhyay,[1] Sarathlal Koyiloth Vayalil,[1] Dominik Graulich,[2] Imran Ahamed,[3] Sonia Francoual,[4] Arti Kashyap,[3] Timo Kuschel,[2] and P. S. Anil Kumar[1,*]

[1]*Department of Physics, Indian Institute of Science, Bangalore 560012, India*

[2]*Center for Spinelectronic Materials and Devices, Department of Physics, Bielefeld University, Universitätsstraße 25, 33615 Bielefeld, Germany*

[3]*School of Basic Sciences & School of Computing and Electrical Engineering, Indian Institute of Technology, Mandi 175005, India*

[4]*Deutsches Elektronen-Synchrotron DESY, Notkestraße 85, 22607 Hamburg, Germany*

(Received 19 October 2019; revised 3 October 2020; accepted 5 October 2020; published 23 October 2020)

The magnetic proximity effect in top and bottom Pt layers induced by Co in Ta/Pt/Co/Pt multilayers has been studied by interface-sensitive, element-specific x-ray resonant magnetic reflectivity. The asymmetry ratio for circularly polarized x-rays of left and right helicity has been measured at the Pt L_3 absorption edge (11 567 eV) with an in-plane magnetic field ($\pm$158 mT) to verify its magnetic origin. The proximity-induced magnetic moment in the bottom Pt layer decreases with the thickness of the Ta buffer layer. Grazing incidence x-ray diffraction has been carried out to show that the Ta buffer layer induces the growth of Pt(011) rather than Pt(111), which in turn reduces the induced moment. A detailed density functional theory study shows that an adjacent Co layer induces more magnetic moments in Pt(111) than in Pt(011). The manipulation of the magnetism in Pt by the insertion of a Ta buffer layer provides a way to control the magnetic proximity effect, which is of huge importance in spin-transport experiments across similar kinds of interfaces.

DOI: 10.1103/PhysRevB.102.144435

I. INTRODUCTION

Interfacial spin-orbit coupling in ferromagnet-nonmagnet (FM/NM) systems promotes remarkable spin-related phenomena and interactions such as the interfacial spin Hall effect [1–4], the interfacial Dzyaloshinskii-Moriya interaction (iDMI) [5–7], the Rashba effect [8,9], and spin-orbit torque (SOT) [10,11]. All of these effects simultaneously provide the electrical manipulation of the magnetization to control magnetization switching by current-driven domain wall motion. A static magnetic moment in the adjacent NM can be induced by the FM in certain FM/NM systems (e.g., Fe/Pd, Fe/Pt) [12,13]. The phenomenon of a nominally paramagnetic material getting spin-polarized in the presence of an adjacent FM or ferrimagnetic material by the exchange interaction is known as the magnetic proximity effect (MPE) [14,15]. This effect can be commonly observed in materials such as Pt, which is a Pauli paramagnet following the Stoner criterion [16].

The MPE must be investigated to understand the magnetic properties of the atoms near the FM/NM interface. Earlier studies have shown that the structural properties of the atoms near the FM/NM interface determine the spin-transport properties [17,18]. Furthermore, broken spatial inversion symmetry at the FM-NM interface can be attributed to nonequivalent spin-transport properties (e.g., SOT, iDMI) [19–22] between NM/FM (FM on top of NM) and FM/NM (NM on top of FM). Earlier studies showed that in symmetric NM/FM/NM systems, SOT and iDMI can prevail due to different structural and/or magnetic properties at the NM/FM and FM/NM interfaces.

MPE has been experimentally reported [23–31] mainly using x-ray magnetic circular dichroism (XMCD). In the presence of FM metals such as Fe [26], Ni [27,28], and Co [29–31], Pt has been reported to be spin-polarized, and the absolute magnetic moment per Pt atom has been quantified using the XMCD sum rules in those Pt/FM bi- and multilayer systems. The XMCD technique becomes insensitive in extracting the absolute magnetic moment per atom of a specific element at buried interfaces in a multilayer thin film system [32]. In the XMCD technique, the signal is averaged over the total thickness of a layer, but due to MPE only a part of the total thickness of an NM layer becomes spin-polarized, which actually contributes to the XMCD signal. Hence, the XMCD technique fails to measure the absolute magnetic moment of the partly spin-polarized NM layer, at least within a single sample. Only analyzing a NM-thickness-variation series can help to get a depth analysis of the magnetic NM moment solely by XMCD [28,30,31], which is much more effort than just obtaining the magnetic depth profile from a single sample. Compared to XMCD, another technique, namely x-ray resonant magnetic reflectivity (XRMR), depends on the spin-dependent interference of x-rays reflected from the interfaces of a multilayer [33]. Depending on the energy of the x-rays used, the XRMR technique can detect the magnetic properties of multilayers with element- and depth-sensitivity.

In this work, the induced spin polarization in the top and bottom Pt layers due to the Co layer in Ta/Pt/Co/Pt

*anil@iisc.ac.in

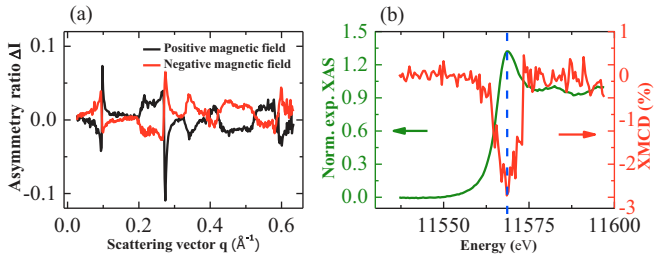

FIG. 1. (a) XRMR asymmetry ratio $\Delta I(q)$ for both magnetic-field directions at the resonant energy of 11 567 eV. (b) Experimental energy-dependent XAS spectrum (green curve) and the XMCD signal (red curve). All data correspond to the Ta(2 nm)/Pt(4 nm)/Co(2 nm)/Pt(2 nm) multilayer.

multilayers grown on Si/SiO_2 substrate has been investigated. We used the XRMR technique to quantify the magnetic moments in the two different Pt layers of the multilayer, and we found that the top Pt layer has a larger induced magnetic moment than the bottom one that is adjacent to the Ta buffer layer. Furthermore, the induced magnetic moment in the bottom Pt layer reduces with increasing thickness of the Ta buffer layer. We have observed that the Ta buffer layer favors the growth of Pt(011) rather than Pt(111). Hence, by varying the thickness of the Ta buffer layer, the growth of the Pt layer can be modified, which in turn can control the MPE in the Pt layer due to the Co layer. Kuschel *et al.* showed that the effective spin-polarized Pt thickness is independent of the thickness of the Pt layer by investigating FM/Pt bilayer systems [13]. In this work, we confirm this independence for Pt/FM/Pt multilayer systems. Experimental results are also compared with density functional theory calculations. In addition, the magnetic moment values observed by the XRMR technique are found to be comparable with the results obtained from a vibrating sample magnetometer (VSM).

II. EXPERIMENT

Ta(t)/Pt(4)/Co(2)/Pt(2) multilayers (all the thicknesses are in nm) have been deposited by dc magnetron sputter deposition on Si substrates with a 285 nm amorphous SiO_2 layer (3.8×3.8 mm^2). The thickness of the Ta buffer layer (t) has been varied from 0 to 10 nm, where zero indicates the multilayer without any Ta buffer layer. The multilayers with $t = 0$, 2, 4, 7, and 10 nm have been designated as S1, S2, S3, S4, and S5, respectively. The multilayer Ta(3)/Pt(2)/Co(2)/Pt(2) (all the thicknesses are in nm) has been designated as S6. The deposition has been done at room temperature (RT) with an argon pressure of 5×10^{-3} mbar in a high vacuum chamber with a base pressure below 5×10^{-8} mbar. The deposition rates of Ta, Pt, and Co were 0.022, 0.047, and 0.023 nm/s, respectively. During deposition, the substrate has been rotated with 30 rotations/min in order to obtain uniform film thicknesses. VSM measurements at RT have been done on the multilayers with an in-plane magnetic field up to ± 1 T.

The XRMR and XMCD measurements were carried out at the resonant scattering and diffraction beamline P09 (EH1) of the third-generation synchrotron PETRA III at DESY (Hamburg, Germany) [34]. A six-circle diffractometer was used to carry out x-ray reflectivity (XRR) scans in θ-2θ scattering geometry. XRMR is based on the magneto-optic change of optical properties of the investigated material. The complex refractive index of a material is given by $n = 1 - \delta + i\beta$, with dispersion coefficient δ and absorption coefficient β, connected via the Kramers-Kronig relation. These coefficients vary by a fraction in magnetic materials depending on the relative orientation of the magnetization with respect to the polarization vector of the incident beam, and these variations are most pronounced at photon energies close to the absorption edge of the specific material. The theoretical background of XRMR has been described in Ref. [33] in detail.

The fundamental aspect of XRMR is to determine the depth profile of the magneto-optic parameters $\Delta\delta$ and $\Delta\beta$, which correspond to the magnetic change of the dispersion δ and absorption β coefficients, respectively. In our case, the XRR was measured at an off-resonant energy (11 467 eV) and at the resonant energy (11 567 eV) close to the white line of the Pt L_3 absorption edge in the presence of an in-plane permanent magnet with a magnetic field of 158 mT at RT. The degree of circular polarization of the incident x-rays was 92 ± 3 % as determined using an Au (111) analyzer crystal. A single 850-μm-thick diamond plate at quarter wave plate condition was used to produce incident circularly polarized light. The reflected intensity of left (I_L) and right (I_R) helicity for each scattering vector **q** (XRMR) and energy (XMCD) was determined by switching fast the helicity of the incident circular polarization and averaging.

Afterwards, the XRMR asymmetry ratio $\Delta I = (I_L - I_R)/(I_L + I_R)$ was calculated from the collected data and fitted with an appropriate model. All the data processing and fitting have been done using the ReMagX analysis tool [35] following the recipe provided by Klewe *et al.* [32]. The fitting algorithm for the nonmagnetic reflectivity data is based on the recursive Parratt formalism [36] with roughness described by the Névot-Croce approximation [37]. The fitting algorithm for the asymmetry ratio is based on the Zak matrix formalism [38]. The tool models and varies the magneto-optic depth

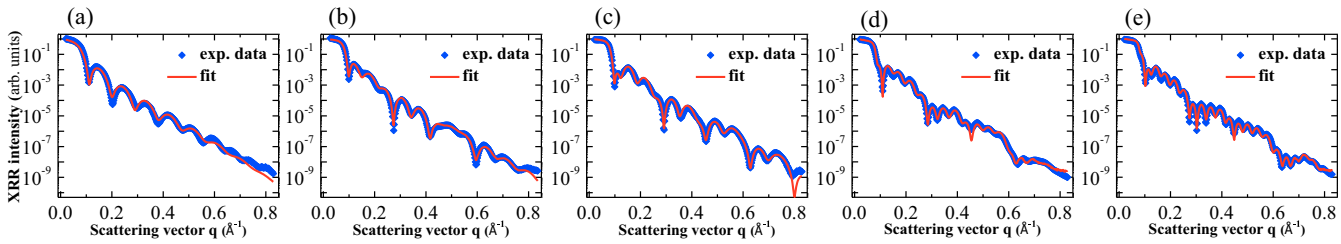

FIG. 2. (a)–(e) The off-resonant (11 467 eV) averaged XRR signals with fits for all the multilayers.

TABLE I. Structural parameters, thickness t, and roughness σ expressed in nm of all the layers in each multilayer.

Multilayer	t SiO_2	σ bulk/Ta	t Ta	σ Ta/Pt	t Pt	σ Pt/Co	t Co	σ Co/Pt	t Pt	σ Co/Pt
S1	bulk		0 (without Ta)	0.49 (SiO_2/Pt)	**3.40**	1.00	**1.63**	0.58	**1.60**	0.32
S2	bulk	0.47	**2.18**	0.29	**3.65**	0.32	**2.16**	0.35	**1.59**	0.42
S3	bulk	0.46	**3.68**	0.33	**3.69**	0.35	**1.66**	0.49	**1.81**	0.35
S4	bulk	0.49	**6.67**	0.38	**3.71**	0.39	**1.57**	0.42	**1.92**	0.37
S5	bulk	0.42	**10.20**	0.59	**3.37**	0.35	**1.57**	0.44	**1.90**	0.36
S6	bulk	0.52	**3.00**	0.37	**2.04**	0.42	**1.97**	0.38	**1.77**	0.39

profiles, i.e., the in-depth distributions of $\Delta\delta$ and $\Delta\beta$, while keeping the absolute values for δ and β unchanged. In the matrix formalism, the roughness is also treated as an optical profile with a Gaussian-like distribution centered at the interface. The magneto-optic depth profile has been converted to Pt magnetic moment (μ_B/Pt) using the conversion factor obtained by *ab initio* calculations [13].

The XMCD spectrum was collected using an energy-dispersive silicon drift detector (VORTEX) synchronized with the piezoactuators underneath the phase plates, thus allowing for the fluorescent photons for left and right circularly polarized incident beams to be counted separately at every point of the scan.

The XRMR asymmetry ratio plotted against the scattering vector $q = \frac{4\pi \sin\theta}{\lambda}$ has been plotted in Fig. 1(a) for S2. The profile changes the sign with the reversal of the magnetic field direction, which confirms its magnetic origin.

III. RESULTS AND DISCUSSION

The experimental energy-dependent x-ray absorption spectrum (XAS) at the Pt L_3 edge normalized to the edge jump [green curve in Fig. 1(b) for S2] has been depicted along with the XMCD intensity [red curve in Fig. 1(b) for S2] to identify the energy with maximum dichroism. It can be confirmed that the maximum dichroism is close to the white-line intensity of the L_3 absorption edge [24] comparable to recent *ab initio* calculations [13] and experimental studies using fixed-q scans [39] and XMCD [40]. We have chosen the resonant energy 11 567 eV for collecting the XRMR data. The white-line intensity (ratio of absorption maximum and edge jump) is 1.32, which indicates the metallic states of Pt (1.25 for metallic Pt, 1.50 for $PtO_{1.36}$, and 2.20 for $PtO_{1.6}$) [41].

The footprint-corrected normalized XRR signal of the multilayer collected at an off-resonant photon energy of 11 467 eV has been plotted against the scattering vector q [see Figs. 2(a)–2(e)]. The structural parameters have been obtained by fitting the off-resonant XRR data of each multilayer using the Parratt formalism, and they are tabulated in Table I. After determining the layer thicknesses and interlayer roughnesses in a certain multilayer by the off-resonant fit (11 467 eV), the averaged resonant (11 567 eV) XRR curve has been fitted [indicated in Figs. 3(a)–3(e)] with the fixed structural parameters to obtain the optical parameters δ and β of all the layers. The structural

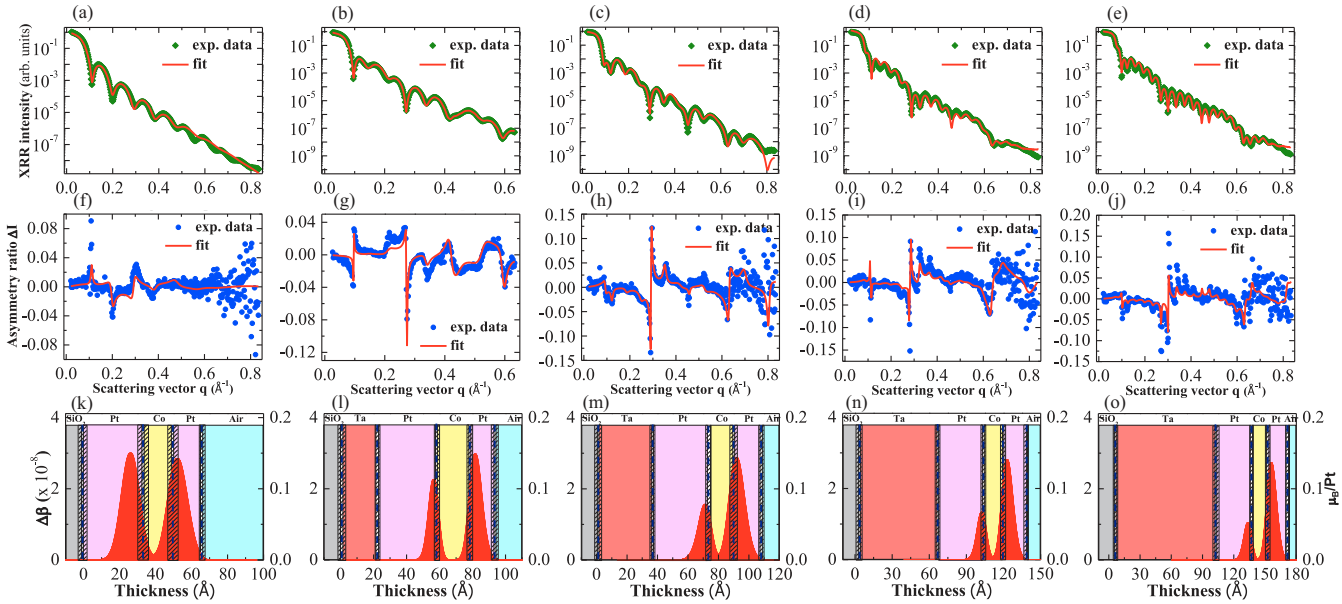

FIG. 3. (a)–(e) The resonant (11 567 eV) averaged XRR signals with fits. (f)–(j) The corresponding measured and fitted XRMR asymmetry ratios $\Delta I(q)$ for the multilayers. (k)–(o) Magneto-optic depth profiles, which were used to fit the XRMR asymmetry ratios. Red histograms depict the in-depth distribution of the spin-polarized Pt atoms. The induced magnetic moment per Pt atom has been quantified from *ab initio* calculation. The dashed lines denote the corresponding interface position between the layers, whereas the dashed rectangles between the layers denote the corresponding interlayer roughness.

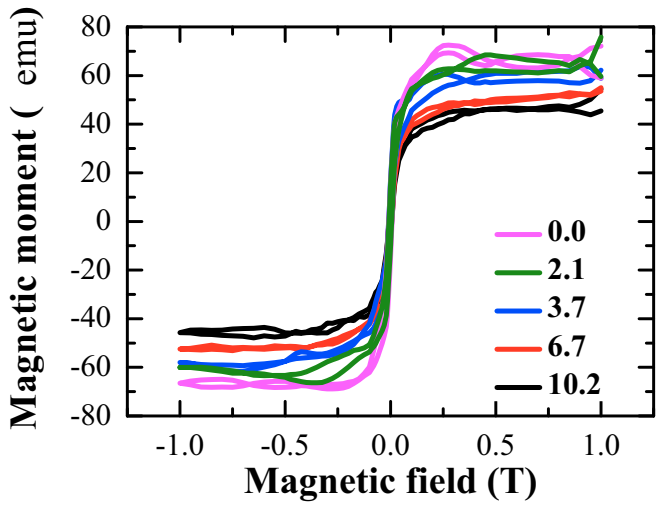

FIG. 4. Vibrating sample magnetometer measurement of the Ta(t)/Pt(4 nm)/Co(2 nm)/Pt(2 nm) multilayers in in-plane geometry.

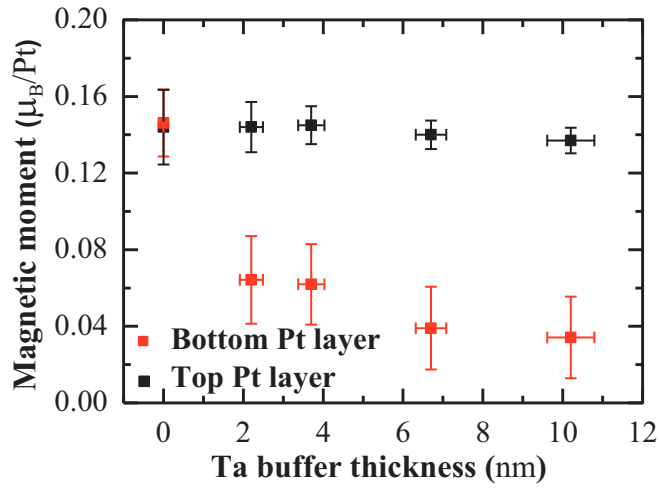

FIG. 5. Dependence of magnetic moment in the top and bottom Pt layers on the Ta buffer thickness.

parameters obtained from the off-resonant XRR fit and the optical parameters obtained from the resonant XRR fit have been used to fit the XRMR asymmetry ratio by varying only the $\Delta\beta$ depth profile, keeping $\Delta\delta$ at zero. In earlier studies [13,32], it was shown theoretically by Kuschel *et al.* and experimentally by Klewe *et al.* that for the Pt absorption edge, $\Delta\delta$ becomes zero at the maximum of $\Delta\beta$. The measured XRMR asymmetry ratios for the multilayers are shown in Figs. 3(f)–3(j) accompanied by their respective fittings. The magneto-optic depth profiles of $\Delta\beta$ are shown in Figs. 3(k)–3(o). These profiles were generated by a Gaussian function at each of the Pt/Co interfaces, convoluted with the roughness profiles of the respective interface [32].

The full width at half-maximum (FWHM) of these Gaussian-like profiles has been calculated to quantify the effective thickness of spin-polarized Pt layers at the two interfaces. By comparing the experimental fit values of $\Delta\beta$ with the *ab initio* calculations [13], the magnetic moment per spin-polarized Pt atom at the maximum of these profiles has been determined. The magnetic moment contribution m_{XRMR} from the Co layer with a saturation magnetization of 1400 emu/cm^3 at RT [42] and the two Pt layers in a certain multilayer has been calculated by determining the area under the curve of the magneto-optic profiles. The saturation magnetic moments m_{VSM} for all the multilayers have been extracted from their respective VSM measurements at RT (see Fig. 4). All the relevant extracted data have been summarized in Table II. It can be readily seen from Table II that m_{XRMR} and m_{VSM} are very much comparable. Hence, the total magnetic moment of a NM/FM/NM system can be considered as summation of the magnetic moment of the FM layer and the induced magnetic moment in the NM layer by the FM layer. Hence, the enhancement in magnetic moment of a multilayer can be attributed to the MPE.

Comparing the FWHMs of the spatial distribution of the induced magnetic moment due to the MPE, it can be realized that the effective spin-polarized Pt thickness is about 1 nm for all the multilayers (see Table II) and it is independent of the Pt thickness, confirming earlier results [13]. Comparing all the magnetic depth profiles of the spin-polarized Pt layers, it can be realized that the maximum induced magnetic moment per Pt atom in the bottom Pt layer decreases with the increase in thickness of the Ta buffer layer (see Fig. 5). Moreover, XRMR has also been carried out on S6 [see Fig. 6(c)]. Due to the Ta buffer layer, the induced magnetic moments in the top and the bottom Pt layers are different, even if the thicknesses of the two Pt layers are the same [see Fig. 6(d)]. It can be readily seen that the magnetic depth profiles of S2 [Fig. 3(l)], S3 [Fig. 3(m)], and S6 [Fig. 6(d)] are similar. It should be noted that the nearly equal roughness at the top Co/Pt and bottom Pt/Co interfaces reduces the possibility of different intermixing at the top and bottom Co/Pt interfaces to get different

TABLE II. $\mathbf{m}_{\mathrm{Co}}$, $\mathbf{m}_{\mathrm{Pt}}^{\mathrm{bottom}}$, and $\mathbf{m}_{\mathrm{Pt}}^{\mathrm{top}}$ represent the magnetic moment in the Co layer, the bottom, and the top Pt layer, respectively. $\mathbf{m}_{\mathrm{XRMR}}$ and $\mathbf{m}_{\mathrm{VSM}}$ denotes the total magnetic moment of the multilayer measured by XRMR and VSM, respectively. t^{spin} represents the spin-polarized thickness of the Pt layers.

Multilayer	$\mathbf{m}_{\mathrm{Co}}$ (μemu)	$\mathbf{m}_{\mathrm{Pt}}^{\mathrm{bottom}}$ (μemu)	$\mathbf{m}_{\mathrm{Pt}}^{\mathrm{top}}$ (μemu)	$\mathbf{m}_{\mathrm{XRMR}}$ (μemu)	$\mathbf{m}_{\mathrm{VSM}}$ (μemu)	$t^{\mathrm{spin}}_{\mathrm{bottom\ Pt}}$ (nm)	$t^{\mathrm{spin}}_{\mathrm{top\ Pt}}$ (nm)
S1	33.0±0.2	16.1±1.9	14.5±1.9	63.6±4.0	67.0±5.5	1.30	1.24
S2	43.7±0.2	6.7±2.4	11.7±1.1	62.1±3.7	64.5±6.0	0.94	0.98
S3	33.6±0.2	6.5±2.2	13.7±0.9	53.8±3.3	59.5±4.3	1.10	1.17
S4	31.7±0.2	4.5±2.5	13.1±0.7	49.3±3.4	51.0±4.6	0.95	1.13
S5	31.7±0.2	4.1±2.6	13.1±0.6	48.9±3.4	46.0±4.8	0.97	1.21

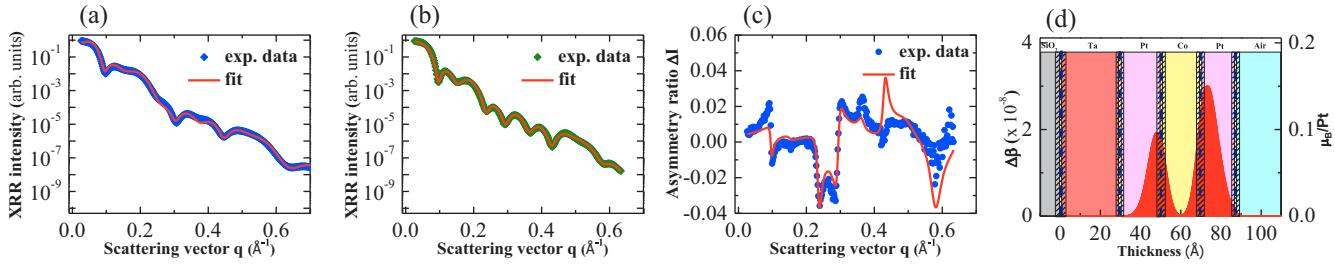

FIG. 6. (a) The off-resonant (11 467 eV) averaged XRR signals with fits; (b) the resonant (11 567 eV) averaged XRR signals with fits; (c) the corresponding measured and fitted XRMR asymmetry ratio $\Delta I(q)$ for the Ta(3)/Pt(2)/Co(2)/Pt(2) multilayer; (d) magneto-optic depth profile, which was used to fit the XRMR asymmetry ratio. Red histograms depict the in-depth distribution of the spin-polarized Pt atoms. The induced magnetic moment per Pt atom has been quantified from *ab initio* calculation. The dashed lines denote the corresponding interface position between the layers, whereas the dashed rectangles between the layers denote the corresponding interlayer roughness.

MPE in the two Pt layers (see Table I). In general, a change in δ and β at the interfaces can be induced by roughness or by intermixing. However, due to the described deposition condition, a significant intermixing is very unlikely. Also the maximum induced magnetic moment in Pt, observed by us, is in good agreement with the size of the induced moment in chemically separated Co/Pt layered structures and significantly smaller than expected for CoPt alloys [24]. Therefore, there is a strong possibility that the observed difference in moment may be due to a difference in the structural properties between the two Pt layers. Obviously, the structural properties of the bottom Pt layer deposited on the Ta buffer layer could be different from that of the top Pt layer deposited on the Co layer due to different growth ambience [43].

It is interesting to note that in recent years, hard XRMR studies on trilayer systems have been reported for Pt/Co/Pt [20], Pt/CoFeTaB/Pt [44], and Pd/Co/Pd [45]. It has been shown qualitatively that the top NM layer has an enhanced induced magnetic moment compared to the bottom one. Inyang *et al.* [44] have shown that the different local magnetization of CoFeTaB has produced the different induced magnetic moment in Pt layers in the CoFeTaB/Pt and Pt/CoFeTaB interfaces. Such local magnetization of Co should not differ significantly between the Pt/Co and Co/Pt interfaces. Hence, it is important to understand the origin of such an observation. Therefore, we deposited Ta(t)/Pt(4 nm) bilayers on the same substrate under the same growth condition. Grazing incidence x-ray diffraction has been carried out on these bilayers with an incidence angle of 0.5° (see Fig. 7) to get more structural information of the bottom Pt layer. It has been observed that with larger Ta thickness, the growth of Pt(011) becomes more prominent than Pt(111). Similar growth has been observed in our recent work [46]. X-ray diffraction (XRD) has been carried out on these bilayers (shown in the supplemental

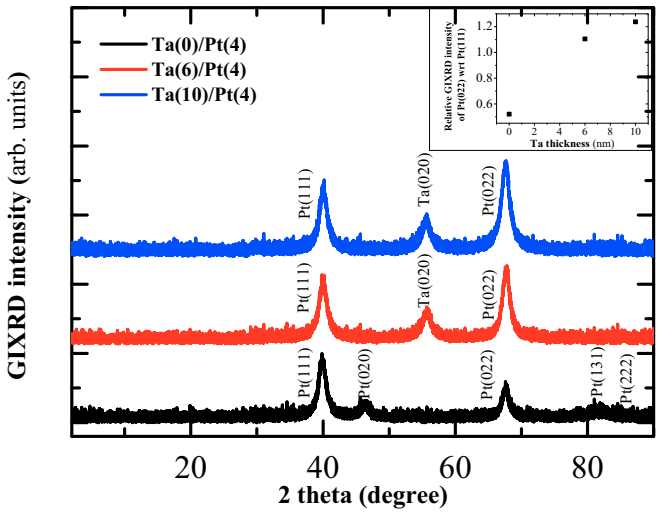

FIG. 7. Grazing incidence x-ray diffraction data with an incidence angle of 0.5° of Ta(t)/Pt(4 nm) bilayers with t = 0, 6, and 10 nm. Data have been vertically shifted with an offset for a better view. The inset shows the relative intensity ratio of Pt(022) with respect to Pt(111).

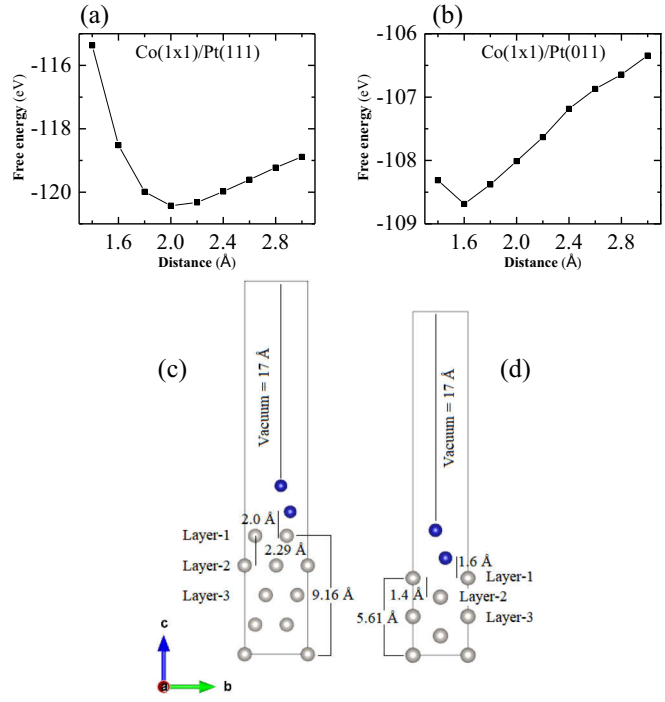

FIG. 8. The free-energy variation with the separation between Co and Pt layers in (a) Co(1×1)/Pt(111) and (b) Co(1×1)/Pt(011), respectively. The modeled bilayers of Co/Pt as (c) Co (1×1) on Pt(111) and (d) Co (1×1) on Pt(011). Gray and blue atoms are Pt and Co, respectively.

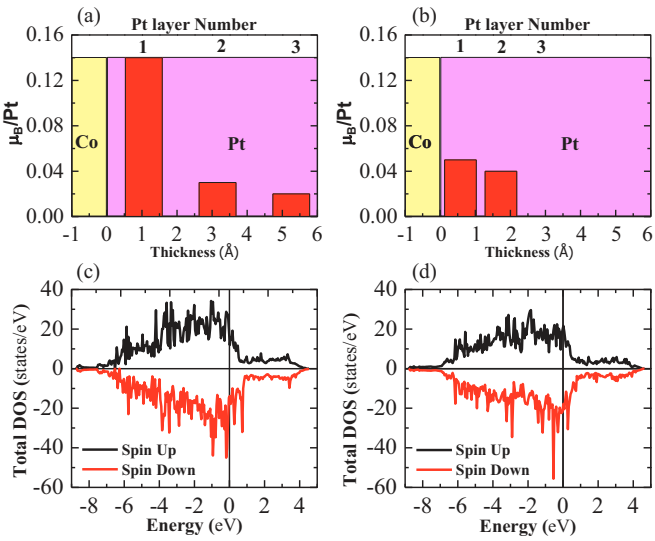

FIG. 9. Layerwise variation of the induced magnetic moment (a) Co/Pt(111) and (b) Co/Pt(011) systems is presented. The total density of states of (c) Co/Pt(111) and (d) Co/Pt(011) systems is shown.

material [47]). The XRD scans ranging from 60° to 75° have been fitted using pseudo-Voigt functions, which shows that the XRD intensity of Pt(011) at 67.6° increases with increasing thickness of the Ta buffer layer (shown in the supplemental material [47]).

We have done density functional theory calculations to compare between Co/Pt(111) and Co/Pt(011) interfaces. As the Ta buffer layer only modifies the crystallinity of the bottom Pt layer, the Co/Pt interface is modeled accordingly. Here, Pt(111) and Pt(011) have been taken as substrates, and ionic relaxation was performed for both Pt substrates. A Co supercell of 1×1 was placed on top of both Pt(111) and Pt(011) substrates, and vacuum of 17 Å was provided along the z-direction. The modeled Co/Pt(111) and Co/Pt(011) bilayers with optimized separation between Co and Pt layers are shown (see Fig. 8). In the modeled bilayers, only Co atoms were allowed to relax in the x-y plane with optimized z. We have used DFT as employed in the Vienna Ab initio Simulation Package [48–50] to study the electronic structure and magnetic properties of the Co/Pt bilayers. Furthermore, a Perdew-Burke-Ernzerhof-based [51] spin-polarized semilocal exchange-correlation functional was used. Projected augmented wave [50,52] method-based potentials have been used for both Co and Pt atoms. The valence electrons taken for the Co atoms and the Pt atoms were d^8s^1 and s^1d^9, respectively. For structural optimization, Gaussian smearing was used with a Monkhorst-Pack (MP) [53] **k**-mesh of $3 \times 5 \times 1$. The accurate calculation of electronic structure was carried out with tetrahedron smearing using a finer MP **k**-mesh of $5 \times 11 \times 1$ and $5 \times 13 \times 1$ for Co/Pt(111) and Co/Pt(011) bilayer systems, respectively. The convergence criteria for forces on each atom in the structural optimization and for the electronic self-consistency were set to 0.0005 eV/Å and 10^{-7} eV, respectively. The variations of the induced magnetic moment due to the Co atoms on the Pt atoms for both crystal structures in various layers are presented in Figs. 9(a) and 9(b) for Co/Pt(111) and Co/Pt(011), respectively. It can be seen that the induced magnetic moments are $0.14\mu_B$/Pt and $0.05\mu_B$/Pt at the interfaces of Co/Pt(111) and Co/Pt(011), respectively.

Any difference in the structural or magnetic properties at the interface can impact the MPE to modify the spin-transport phenomena [17,18] in NM/FM/NM systems. As the MPE originates from the $3d$-$4d$ or $3d$-$5d$ [29] hybridization, it can significantly affect the spin-transport properties in NM-FM systems, which are sensitive to the interfacial spin-orbit coupling. Moreover, the asymmetry in the induced magnetic region of NM/FM and that of FM/NM can be manipulated to control the spin-dependent transport phenomena in spin-orbitronic devices [54].

IV. CONCLUSION

In conclusion, we investigated the magnetic proximity effect due to Co layer in two Pt layers of Ta/Pt/Co/Pt multilayers using XRMR. Analyzing the XRMR asymmetry ratio, it has been realized that the values of the induced magnetic moments in the top and bottom Pt layers are different irrespective of their structural thickness and interfacial roughness. The difference in the induced magnetic moment can give rise to various spin-transport phenomena such as SOT and iDMI. The Ta buffer layer promotes the growth of Pt(011) rather than Pt(111) as its thickness increases. Density functional theory calculations show that indeed the Pt(111) layer has more induced magnetic moments than the Pt(011) layer has due to the proximity of the Co layer. Moreover, it has been established that the magnetic moment of a multilayer is the summation of the moment in the FM layer and the moment induced by the FM layer in the adjacent NM layers.

ACKNOWLEDGMENTS

The major part of this work was carried out at the light source PETRA III, DESY, a member of the Helmholtz Association (HGF). We would like to thank David Reuther and Philipp Glaevecke, beamline engineer at the P09 beamline, PETRA III at DESY, for the technical support. Financial support by the Department of Science and Technology, Ministry of Science and Technology, India provided within the framework of the India@DESY collaboration and Deutsche Forschungsgemeinschaft within the individual grant (Grant No. RE 1052/42-1) is gratefully acknowledged. A.M. and S.K.V. thank MoE, India and DST-INSPIRE Faculty fellowship respectively, for the financial support.

A.M. and S.K.V. contributed equally to this work.

[1] M. I. Dyakonov and V. I. Perel, Phys. Lett. A **35**, 459 (1971).
[2] S. Zhang, Phys. Rev. Lett. **85**, 393 (2000).
[3] L. Wang, R. J. H. Wesselink, Y. Liu, Z. Yuan, K. Xia, and P. J. Kelly, Phys. Rev. Lett. **116**, 196602 (2016).

[4] J. Sinova, S. O. Valenzuela, J. Wunderlich, C. H. Back, and T. Jungwirth, Rev. Mod. Phys. **87**, 1213 (2015).

[5] I. E. Dzyaloshinskii, J. Expt. Theor. Phys. (U.S.S.R.) **32**, 1547 (1957) [Sov. Phys. JETP **5**, 1259 (1957)].

[6] T. Moriya, Phys. Rev. **120**, 91 (1960).

[7] R. Lavrijsen, D. M. F. Hartmann, A. van den Brink, Y. Yin, B. Barcones, R. A. Duine, M. A. Verheijen, H. J. M. Swagten, and B. Koopmans, Phys. Rev. B **91**, 104414 (2015).

[8] I. M. Miron, T. Moore, H. Szambolics, L. D. Buda-Prejbeanu, S. Auffret, B. Rodmacq, S. Pizzini, J. Vogel, M. Bonfim, A. Schuhl, and G. Gaudin, Nat. Mater. **10**, 419 (2011).

[9] A. Manchon, H. C. Koo, J. Nitta, S. M. Frolov, and R. A. Duine, Nat. Mater. **14**, 871 (2015).

[10] P. Gambardella and I. M. Miron, Philos. Trans. R. Soc. A **369**, 3175 (2011).

[11] I. M. Miron, K. Garello, G. Gaudin, P.-J. Zermatten, M. V. Costache, S. Auffret, S. Bandiera, B. Rodmacq, A. Schuhl, and P. Gambardella, Nature (London) **476**, 189 (2011).

[12] J. Vogel, A. Fontaine, V. Cros, F. Petroff, J.-P. Kappler, G. Krill, A. Rogalev, and J. Goulon, Phys. Rev. B **55**, 3663 (1997).

[13] T. Kuschel, C. Klewe, J.-M. Schmalhorst, F. Bertram, O. Kuschel, T. Schemme, J. Wollschläger, S. Francoual, J. Strempfer, A. Gupta, M. Meinert, G. Götz, D. Meier, and G. Reiss, Phys. Rev. Lett. **115**, 097401 (2015).

[14] P. K. Manna and S. M. Yusuf, Phys. Rep. **535**, 61 (2014).

[15] M. J. Zuckermann, Solid State Commun. **12**, 745 (1973).

[16] E. C. Stoner, Proc. R. Soc. **165**, 372 (1938).

[17] P. M. Haney, H.-W. Lee, K.-J. Lee, A. Manchon, and M. D. Stiles, Phys. Rev. B **88**, 214417 (2013).

[18] M. Jamali, K. Narayanapillai, X. Qiu, L. M. Loong, A. Manchon, and H. Yang, Phys. Rev. Lett. **111**, 246602 (2013).

[19] W. Zhang, M. B. Jungfleisch, W. Jiang, Y. Liu, J. E. Pearson, S. G. E. Velthuis, A. Hoffmann, F. Freimuth, and Y. Mokrousov, Phys. Rev. B **91**, 115316 (2015).

[20] R. M. Rowan-Robinson, A. A. Stashkevich, Y. Roussigné, M. Belmeguenai, S.-M. Chérif, A. Thiaville, T. P. A. Hase, A. T. Hindmarch, and D. Atkinson, Sci. Rep. **7**, 16835 (2017).

[21] T. A. Peterson, A. P. McFadden, C. J. Palmstrøm, and P. A. Crowell, Phys. Rev. B **97**, 020403(R) (2018).

[22] L. J. Zhu, D. C. Ralph, and R. A. Buhrman, Phys. Rev. B **98**, 134406 (2018).

[23] H. Maruyama, A. Koizumi, K. Kobayashi, and H. Yamazaki, Jpn. J. Appl. Phys. **32**, 290 (1993).

[24] G. Schütz, R. Wienke, W. Wilhelm, W. B. Zeper, H. Ebert, and K. Spörl, J. Appl. Phys. **67**, 4456 (1990).

[25] G. Schütz, R. Wienke, W. Wilhelm, W. Wagner, R. Frahm, and P. Kienle, Physica B **158**, 284 (1989).

[26] W. J. Antel, Jr., M. M. Schwickert, T. Lin, W. L. O'Brien, and G. R. Harp, Phys. Rev. B **60**, 12933 (1999).

[27] F. Wilhelm, P. Poulopoulos, G. Ceballos, H. Wende, K. Baberschke, P. Srivastava, D. Benea, H. Ebert, M. Angelakeris, N. K. Flevaris, D. Niarchos, A. Rogalev, and N. B. Brookes, Phys. Rev. Lett. **85**, 413 (2000).

[28] P. Poulopoulos, F. Wilhelm, H. Wende, G. Ceballos, K. Baberschke, D. Benea, H. Ebert, M. Angelakeris, N. K. Flevaris, A. Rogalev, and N. B. Brookes, J. Appl. Phys. **89**, 3874 (2001).

[29] F. Wilhelm, P. Poulopoulos, A. Scherz, H. Wende, K. Baberschke, M. Angelakeris, N. K. Flevaris, J. Goulon, and A. Rogalev, Phys. Status Solidi A **196**, 33 (2003).

[30] M. Suzuki, H. Muraoka, Y. Inaba, H. Miyagawa, N. Kawamura, T. Shimatsu, H. Maruyama, N. Ishimatsu, Y. Isohama, and Y. Sonobe, Phys. Rev. B **72**, 054430 (2005).

[31] S. Rüegg, G. Schütz, P. Fischer, R. Wienke, W. B. Zeper, and H. Ebert, J. Appl. Phys. **69**, 5655 (1991).

[32] C. Klewe, T. Kuschel, J.-M. Schmalhorst, F. Bertram, O. Kuschel, J. Wollschläger, J. Strempfer, M. Meinert, and G. Reiss, Phys. Rev. B **93**, 214440 (2016).

[33] S. Macke and E. Goering, J. Phys.: Condens. Matter **26**, 363201 (2014).

[34] J. Strempfer, S. Francoual, D. Reuther, D. K. Shukla, A. Skaugen, H. Schulte-Schrepping, T. Kracht, and H. Franz, J. Synch. Radiat. **20**, 541 (2013).

[35] S. Macke, ReMagX, An x-ray magnetic reflectivity tool, www.remagx.org.

[36] L. G. Parratt, Phys. Rev. **95**, 359 (1954).

[37] L. Névot and P. Croce, Rev. Phys. Appl. **15**, 761 (1980).

[38] J. Zak, E. R. Moog, C. Liu, and S. D. Bader, J. Magn. Magn. Mater. **89**, 107 (1990).

[39] T. Kuschel, C. Klewe, P. Bougiatioti, O. Kuschel, J. Wollschl äger, L. Bouchenoire, S. D. Brown, J.-M. Schmalhorst, D. Meier, and G. Reiss, IEEE Trans. Magn. **52**, 4500104 (2016).

[40] P. Bougiatioti, O. Manos, O. Kuschel, J. Wollschl äger, M. Tolkiehn, S. Francoual, and T. Kuschel, arXiv:1807.09032.

[41] A. V. Kolobov, F. Wilhelm, A. Rogalev, T. Shima, and J. Tominaga, Appl. Phys. Lett. **86**, 121909 (2005).

[42] R. I. Allen and F. W. Constant, Phys. Rev. **44**, 228 (1933).

[43] R. Lavrijsen, P. P. J. Haazen, E. Mure, J. H. Franken, J. T. Kohlhepp, H. J. M. Swagten, and B. Koopmans, Appl. Phys. Lett. **100**, 262408 (2012).

[44] O. Inyang, L. Bouchenoire, B. Nicholson, M. Tokaç, R. M. Rowan-Robinson, C. J. Kinane, and A. T. Hindmarch, Phys. Rev. B **100**, 174418 (2019).

[45] D.-O. Kim, K. M. Song, Y. Choi, B.-C. Min, J.-S. Kim, J. W. Choi, and D. R. Lee, Sci. Rep. **6**, 25391 (2016).

[46] V. M. Parakkat, K. R. Ganesh, and P. S. Anil Kumar, AIP Adv. **6**, 056118 (2016).

[47] See Supplemental Material at http://link.aps.org/supplemental/10.1103/PhysRevB.102.144435 for the x-ray diffraction (theta-2theta) data of $Ta(t)/Pt(4\ \mathrm{nm})$ bilayers with $t = 0$, 6, 10 nm, respective fits using Pseudo-Voigt functions and the comparison of the fitted intensity of the Pt(022) peak at 67.6° for different Ta buffer layers.

[48] G. Kresse and J. Furthmüller, Comput. Mater. Sci. **6**, 15 (1996).

[49] G. Kresse and J. Furthmüller, Phys. Rev. B **54**, 11169 (1996).

[50] G. Kresse and D. Joubert, Phys. Rev. B **59**, 1758 (1999).

[51] J. P. Perdew, K. Burke, and M. Ernzerhof, Phys. Rev. Lett. **77**, 3865 (1996).

[52] P. E. Blöchl, Phys. Rev. B **50**, 17953 (1994).

[53] H. J. Monkhorst and J. D. Pack, Phys. Rev. B **13**, 5188 (1976).

[54] R. Ramaswamy, J. M. Lee, K. Cai, and H. Yang, Appl. Phys. Rev. **5**, 031107 (2018).